Optimum selective emitters for efficient thermophotovoltaic conversion

Cite as: Appl. Phys. Lett. **116**, 023903 (2020); https://doi.org/10.1063/1.5131367 Submitted: 11 October 2019 . Accepted: 26 December 2019 . Published Online: 13 January 2020

Sakib Hassan, Chloe F. Doiron 🗓, and Gururaj V. Naik 🗓









Publishing



Optimum selective emitters for efficient thermophotovoltaic conversion

Cite as: Appl. Phys. Lett. **116**, 023903 (2020); doi: 10.1063/1.5131367 Submitted: 11 October 2019 · Accepted: 26 December 2019 · Published Online: 13 January 2020







Sakib Hassan, Chloe F. Doiron, Daid Gururaj V. Naik la

AFFILIATIONS

- ¹Department of Electrical and Computer Engineering, Rice University, Houston, Texas 77005, USA
- ²Applied Physics Graduate Program, Smalley-Curl Institute, Rice University, Houston, Texas 77005, USA

ABSTRACT

Though thermophotovoltaic (TPV) systems have been studied for many decades, the demonstrated conversion efficiencies have remained far lower than the theoretical maximum. Here, in this work, we investigate the reason for low efficiency, especially in TPV systems employing selective thermal emitters, and determine design pathways toward high efficiency. We model both the optical and optoelectronic components of the TPV system and study the influence of the emitter selectivity on the optimum bandgap of the photovoltaic cell, heat sink requirements, and maximum conversion efficiency for any given emitter temperature from 1000 to 2000 K. Our calculations suggest that thermal emitters with at least 20 dB suppression of sub-bandgap emission and an emission enhancement of $100 \times can$ push the overall efficiency to 70% of Carnot's limit. Furthermore, we show that such an extreme requirement on suppression is at the performance limits for resonant thermal emitters employing refractory plasmonic materials such as Mo, W, Ta, TiN, and carbon nanotubes.

Published under license by AIP Publishing. https://doi.org/10.1063/1.5131367

Thermophotovoltaic (TPV) devices convert thermal energy radiated from a hot emitter directly into electrical energy without any moving parts. They are compact and lightweight systems capable of operating with various heat sources, including low-grade waste heat.²⁻ Hence, TPV systems are promising for applications, especially in energy, defense, and space.5 TPV systems have been studied for many decades, and yet their conversion efficiencies remain low. 4,6,7 A TPV system can be broken into optical and photovoltaic (PV) subsystems. The optical subsystem controls the spectral or spatial properties of thermal emission for the TPV system. Previous demonstrations have shown that the optical subsystem can be directly integrated into a PV cell through the addition of spectral filters^{8,9} or the use of the PV cell as a spectral filter. 10 To improve the conversion efficiency of TPV systems, both the optical and PV subsystems need to be optimized. A recent report focused on the photovoltaic subsystem demonstrating efficient PV conversion when illuminated by a blackbody source at 1500 K.¹⁰ Nanophotonics provides a route to enhance the optical subsystem by designing an optimal selective thermal emitter. Using nanophotonic design principles, many recent reports demonstrate spectrally selective emitters. 9,11-19 Many of these demonstrations are performed with selective thermal emitters that have near unity thermal emission. Despite achieving selective thermal emitters with near unity peak emissivity, the conversion efficiency of TPV demonstrations remains

relatively low^{15,20} with some of the highest efficiency TPV devices using graybody emitters with spectral filtering.^{8,10} The difficulty in optimization of TPV systems can be attributed to the large number of parameters.²¹ While there are numerous studies that seek to optimize TPV systems, ^{20–24} few have analyzed narrow-band selective thermal emitters with extremely large suppression ($\epsilon_{sub-bandgap} < 0.01$). With recent advancements in nanophotonic engineering, narrow-band selective thermal emitters with extremely low sub-bandgap emissivities between 0.01 and 0.10 have been experimentally demonstrated. With further work, even lower sub-bandgap emissivities may be possible.²⁵ Additionally, experimental demonstrations of near-field radiative heat transfer and far-field thermal extractors show that thermal emission can be significantly enhanced.^{26,27} With these advancements in selective thermal emitter performance, optimization of TPV systems with selective emitters with narrow emission windows, extremely low subbandgap emission, and emission enhancement are required. Optimization of such systems provides a pathway for increasing the efficiency of TPV devices.

In this work, we model both the optical and optoelectronic subsystems of a typical TPV system and study the influence of various spectral features of the selective emitter on the optimum PV bandgap, photothermal heating of the PV cell, and the overall TPV efficiency. We consider TPV systems with and without any enhancement. ^{28–33}

^{a)}Electronic mail: guru@rice.edu

Further, we estimate the maximum possible TPV efficiency for resonant selective emitters employing various refractory plasmonic materials. Though a simple Drude model is used to describe IR optical properties of Mo, W, Ta, TiN, and single walled carbon nanotubes (SWCNTs), we believe that our results serve as a design guide to high efficiency TPV systems.

We build the optical and optoelectronic models of a typical TPV system based on the schematic presented in Fig. 1(a). A selective thermal emitter at a fixed temperature T in the range $1000-2000\,\mathrm{K}$ emits photons into a semiconductor photovoltaic (PV) cell with passive cooling to keep the PV cell at a constant temperature of $300\,\mathrm{K}$. The surface of the PV cell is assumed to have an antireflection coating, resulting in no reflection losses. Since most TPV cells are enclosed in a vacuum, we neglect any heat loss by thermal conduction and convection. The enhancement of thermal emission in the desired band could be employed by either geometrical focusing or near-field enhancement. Geometric focusing considers any form of optical concentration, using devices such as a metalens, far-field thermal extractor, or traditional concentration optics to increase the photon flux density in the desired emission band. $^{26,34-38}$

We consider a realistic emission spectrum for the selective emitter shown in Fig. 1(b). The desired emission window spans from E_G to $E_G + \Delta$, where E_G is the bandgap of the PV cell. The peak emissivity in the emission window is ρ . The emission in the undesired part of the spectrum is suppressed by S (dB), where $S=10\log\frac{1}{\zeta}$, with ζ the emissivity in the undesired part of the spectrum. To make our model more complete, we incorporate the emission due to optical phonons in the constituent dielectric materials. The optical phonon emission can originate from the nanophotonic emitter structure or substrates such as CaF₂ or MgF₂. The emission profile is modeled using a rectangular emission window with bandwidth Δ_{PhP} and the same peak amplitude of ρ . However, while the power transfer in the phonon polaritonic window is small due to low phonon density at the long wavelength region of blackbody emission, the effect is not necessarily negligible.

For the optimization study, we choose the properties of the selective thermal emitter to be within practical limits. We assume that the emitter is made out of metallic/dielectric resonators. IR emission suppression depends on the high temperature optical properties of the material, and we set the maximum suppression to 30 dB since a suppression of 20 dB has been experimentally demonstrated and 30 dB is achievable by a careful nanophotonic design. We fix the bandwidth

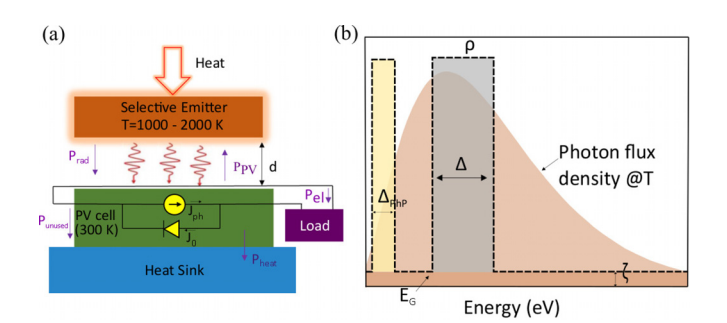


FIG. 1. (a) Schematic of a TPV system consisting of a selective emitter held at a constant temperature in the range of 1000–2000 K and a PV cell maintained at 300 K. (b) Engineered emissivity spectrum of a typical selective emitter, where ρ and ζ are the emissivities in the desired and undesired emission windows.

and the center wavelength of the optical phonon emission window to 3 μ m and 30 μ m, respectively, typical for common infrared dielectrics such as CaF₂.³⁹ We set the single pass absorption length of photons in the PV cell, $t=100~\mu$ m. With the assumption of a perfect back reflector, the total absorption length for photons in the semiconductor is 2t. Above the bandgap, the absorption coefficient α can be given by $\alpha=\alpha_o\sqrt{\hbar\omega-E_G}$, where we set $\alpha_o=6\times10^4{\rm cm}^{-1}$, to reasonably fit to the experimentally measured absorption spectrum of GaSb. Below the bandgap, photons are not absorbed and therefore remain unused. In this analysis, the TPV system considered does not form an optical cavity. Hence, the added benefit of photon recycling is not considered, therefore providing a lower bound on achievable efficiency.

In an ideal PV cell, every superbandgap photon results in an electron-hole pair and the photocurrent J_{ph} , which can be computed using

$$J_{ph} = qc \int_{\omega_{\sigma}}^{\infty} \Theta(\hbar\omega, T) A(\omega) \varepsilon(\omega) d\omega, \tag{1}$$

where ω_g is the frequency corresponding to the bandgap energy, ε is the emissivity spectrum of the selective emitter as shown in Fig. 1(b), c is the speed of light, q is the electronic charge, and $A=1-e^{2\alpha t}$ is the absorptivity. 40 $\Theta(\omega,T)$ is the thermal photon density per frequency at temperature T. Since some part of J_{ph} is lost to carrier recombination, the total current density is $J=J_{ph}-J_r$, where J_r is the recombination current density. The recombination current can arise from radiative, Auger, and trap-assisted recombination, etc., which can be approximated by

$$J_r = J_o \left[\exp\left(\frac{qV}{kT_c}\right) - 1 \right],\tag{2}$$

where V is the bias voltage across the semiconductor p-n junction, k is the Boltzmann constant, T_c is the PV cell temperature (300 K), and J_o is the reverse saturation current density (also called dark current) given by

$$J_o = q \left(\frac{n_i^2 D_h}{N_D \sqrt{\tau_h}} + \frac{n_i^2 D_e}{N_A \sqrt{\tau_e}} \right) + q C n_i^3 t, \tag{3}$$

where the first term accounts for Shockley-Reed-Hall and radiative recombination and the second term represents the Auger recombination loss. The Auger recombination loss (assuming high injection) depends on the bandgap dependent intrinsic carrier concentration, n_i (= $\sqrt{N_c N_v} \exp\left(\frac{-E_G}{2kT}\right)$), and Auger coefficient, C^{40} Here, Q^{20} is the electronic charge, Q^{20} is the diffusion coefficient, Q^{20} is the carrier lifetime, Q^{20} is the doping concentration, Q^{20} is the thickness of the cell, and Q^{20} is the Auger recombination coefficient. By taking the exponential factor out and assuming the values of parameters to be the average of the typically used semiconductor Q^{20} cell (i.e., GaSb, Si, InAs, InGaAs, InSb, etc.), we can approximate the above equation as

$$J_o = 10 \times 10^{10} \exp\left(\frac{-E_G}{kT_c}\right) + qCn_i^3 t,$$
 (4)

where the constant term has units of A/m^2 .

The output electrical power is given by $P_{el} = J_{ph} V_{oc} FF$, where V_{oc} is the open-circuit voltage, J_{sc} is the short-circuit current (V = 0),

and FF is the fill factor. The efficiency (η) is calculated by $\eta = \frac{P_{cl}}{P_{rnd}} \times 100$, where P_{rad} is the radiative power emitted by the emitter. Since the temperature-dependent Carnot efficiency sets an upper bound on the overall TPV efficiency, we express the TPV efficiency as % of Carnot efficiency $(\eta_{carnot} = 1 - T_c/T)$ and denote it as normalized efficiency, η_{norm} . Thus, using normalized efficiency facilitates comparisons between TPV systems with different emitter temperatures.

For the subsequent analysis of our TPV system, we consider two cases: thermal emission with and without enhancement. When there is no enhancement, the peak emissivity (ρ) is unity with suppression (S) ranging from 0 to 30 dB. With enhancement, the effective peak emissivity in the desired window can vary from unity to 100. The same suppression range, 0 to 30 dB, is used for the case with enhancement.

To provide a baseline case for analyzing TPV systems with a selective emitter, we calculated the maximum achievable efficiency with an ideal blackbody emitter (without any selectivity) to mimic the Shockley-Queisser limit calculation for TPV systems. As shown in Fig. 2(a), $\eta_{norm,max}$ only reaches 20% even for a 2000 K emitter and $E_G=0.5\,\mathrm{eV}$. The unused sub-bandgap photons and thermalization of the superbandgap photons, together with high dark current in a low bandgap PV cell, are responsible for low efficiencies. Moreover, this implementation results in substantial heating of the PV cell, necessitating significant cooling, an added complexity for system realization. Next, we calculate the same TPV conversion efficiency assuming an "ideal emission spectrum" with an infinite suppression and $\Delta=0.1\,\mathrm{eV}$ [Fig. 2(b)]. We find that η_{norm} can be as high as 60% even with a moderate emitter temperature of 1300 K and E_G of $\sim 1\,\mathrm{eV}$. From this analysis, it is clear that the selectivity of the emitter is the key to a high efficiency operation.

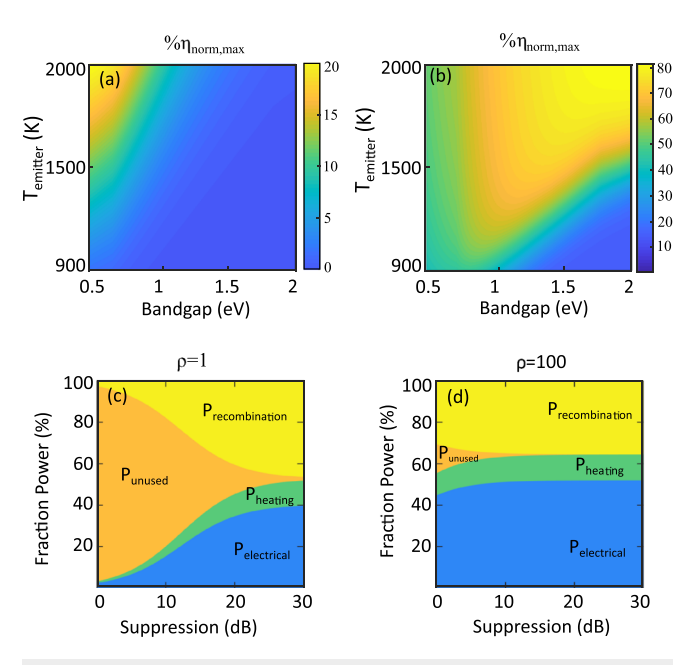


FIG. 2. Maximum achievable efficiency of a far-field TPV system normalized to Carnot's limit for (a) a blackbody emitter and (b) an ideal selective emitter with an infinite suppression of photons in the undesired spectrum. The breakup of the total emitted power vs suppression in a TPV system with (c) no enhancement and (d) with an enhancement of $100\times$. The bandgaps of PV cells are $0.7\,\text{eV}$ for (c) and $0.85\,\text{eV}$ for (d), and the emitter temperature is $1300\,\text{K}$.

A first step toward optimizing the emission profile of the selective emitter is to maximize the emission bandwidth above E_G . Since the dark current of a low bandgap PV cell is large at room temperature, a significant photocurrent is required to reach high efficiency. Thus, the emission bandwidth (Δ) should be wide enough to allow all superbandgap photons to reach the PV cell. While a wide emission window increases efficiency, this comes at the cost of greater thermalization losses, increasing undesirable heating in the PV cell.

The influence of the suppression factor (S) may be seen from Figs. 2(c) and 2(d) for an emitter operating at 1300 K. Using optimum bandgap PV cells, no suppression (S = 0 dB) leads to a large fraction of the total emitted power being unused due to the lack of absorption of sub-bandgap photons [Fig. 2(c)]. Increasing the suppression to 20 dB is necessary to reduce the fraction of unused photons. By increasing the suppression from 0 dB to 20 dB, the unused photon fraction drops from 90% to 20%. While increasing the suppression ratio is a route to increase the efficiency, the final efficiency of the TPV system is limited by the competition between photocurrent and dark current. This competition may be tipped toward a higher efficiency with moderate enhancement as seen in Fig. 2(d). Even with no suppression (S = 0 dB), enhancement increases the fraction of emitted power converted to electrical power. With suppression, the small fraction of unused power from sub-bandgap photons is eliminated. Thus, without any enhancement, suppression is the key to higher efficiency. With a large enhancement such as 100×, the effect of suppression on the overall efficiency is significantly reduced.

The competition between photocurrent and dark current might seem to favor higher efficiencies with a higher bandgap PV cell. However, the exponential dependences of the dark current and the blue edge of the blackbody radiation balance out to give a nearly constant efficiency. Figures 3(a) and 3(b) show the normalized efficiencies

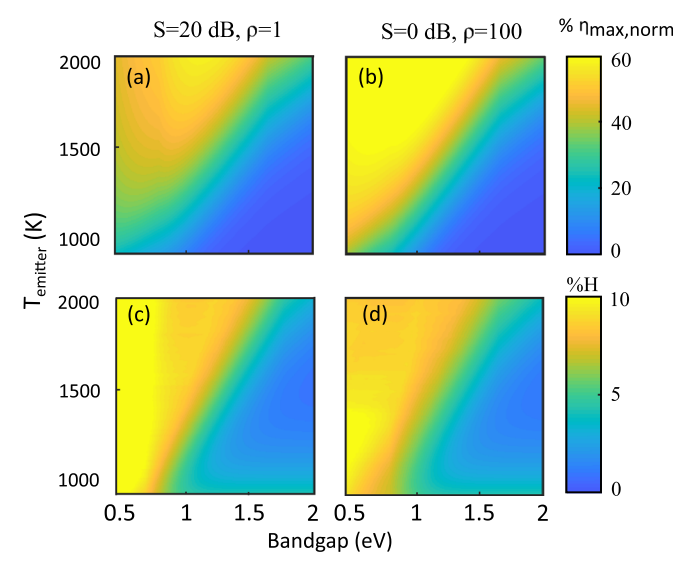


FIG. 3. Maximum possible TPV efficiency normalized to Carnot's limit for a TPV system employing a selective emitter with (a) a 20 dB suppression and no enhancement and (b) no suppression (S = 0 dB) and $100\times$ enhancement. (c) and (d) The corresponding fraction of the emitted power lost as heat (% $H = \frac{P_{heat}}{P_{emitted}} \times 100$) in the same TPV system.

vs PV bandgap calculated for two cases: no enhancement but with a suppression of 20 dB, and enhancement of $100\times$ but without any suppression. With no enhancement, the TPV efficiency is nearly flat in a small range of E_G , and the optimum bandgap ranges from 0.6 to $1.2\,\mathrm{eV}$ for 1000 to $2000\,\mathrm{K}$ emitters, respectively. However, with the enhancement of $100\times$ and no suppression, the efficiency plateau gets wider and the overall conversion efficiency is higher.

While efficiency is an important metric to optimize, reducing heating of the PV cell might be equally important for many applications. Figures 3(c) and 3(d) plot the fraction of total power, resulting in PV cell heating for the same two cases: $\rho=1$ and $S=20\,\mathrm{dB}$ and $\rho=100$ and $S=0\,\mathrm{dB}$. Since the efficiency plateaus around the optimum PV cell bandgap, choosing a higher bandgap within the plateau region reduces heating while incurring negligible loss in efficiency.

From the previous discussion, it is clear that the ultimate efficiency limit of a TPV system depends on the suppression and enhancement factors of the thermal emitter. The maximum achievable conversion efficiencies for emitters at 1300 K with and without suppression are shown in Figs. 4(a) and 4(b). These figures show that without enhancement, a suppression of 20 dB or more is necessary to achieve an overall efficiency of over 40% of Carnot's limit. Similarly, an enhancement of $100\times$ can result in similar efficiency numbers with no suppression (S = 0 dB). However, the simultaneous suppression of

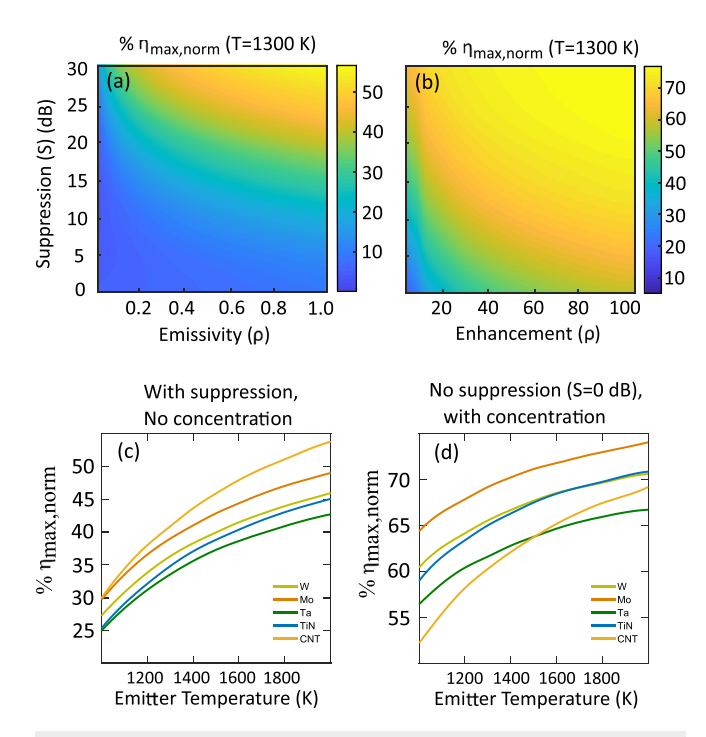


FIG. 4. Maximum possible TPV efficiency normalized to Carnot's limit vs subbandgap suppression and superbandgap enhancement: (a) far-field without enhancement where the enhancement is capped at unity and (b) enhancement or geometric concentration. Estimated trends of TPV efficiency for TPV systems employing resonant selective emitters built from common refractory metals, TiN, and aligned single walled carbon nanotubes (a-SWCNTs). (c) Far-field without any enhancement and (d) near-field enhancement or geometric concentration, but no suppression (S = 0 dB).

20 dB or more and enhancement of $70\times$ or more only can lead to efficiencies of over 70% of Carnot's limit.

Achieving large suppression in a broad spectral range and large enhancement in a narrow band is not easy, especially at high temperatures. All optical materials degrade at high temperatures, resulting in larger absorption losses and poorer light confinement. Since many nanophotonic designs of selective thermal emitters use refractory metals, we estimate an approximate limit to the TPV efficiency imposed by the optical properties of the refractory metals. We consider common refractory metals such as W, Mo, and Ta. Additionally, we examine two recently developed refractory plasmonic materials: TiN⁴¹ and aligned single walled carbon nanotubes (a-SWCNTs). 42 We analyze the system under two common configurations: far-field thermal radiation with suppression, but no enhancement as shown in Fig. 4(c), and near-field thermal radiation with enhancement or concentration, but no suppression (S = 0 dB) as shown in Fig. 4(d). We consider nearfield thermal radiation instead of the geometrical concentration because the near-field configuration has been considered well-suited, especially for compact micro-TPV converters.³⁰ Also, the emitter material parameters have a nontrivial influence on the near-field enhancement.

In these calculations, we make some simple approximations for material-dependent ρ and S and assume that the refractory metals behave as Drude metals. Thus, the results of this analysis are mostly qualitatively significant. Following Ref. 43, for Figs. 4(c) and 4(d), $\zeta \approx \frac{\gamma(T)}{\omega_p(T)}$ and $\rho \approx \frac{\omega_p^2}{\gamma \omega}$. The temperature-dependent Drude parameters for metals are calculated based on the model described in Ref. 44. The room temperature Drude parameters necessary for the model are obtained from Refs. 41, 42, and 45.

From Figs. 4(c) and 4(d), we find that all refractory plasmonic materials allow higher normalized efficiencies at higher operating temperatures. Further, the near-field configuration gives an efficiency boost by about 20–30%. While a-SWCNTs make an excellent refractory material platform for far-field TPV systems, Mo is the best choice for near-field systems. In this analysis, a-SWCNTs are treated as a purely plasmonic material. However, considering their extremely large photonic density of states stemming from hyperbolic dispersion, ⁴² the conversion efficiency for near-field systems could be much higher. Thus, a-SWCNTs are a promising refractory material platform for TPV converters.

In summary, we investigated the impact of selective emission on the overall efficiency of TPV conversion and identified pathways to high efficiency TPV systems. We found that suppression of emission in the sub-bandgap spectrum and enhancement of emission in the superbandgap spectrum are the two key requirements for high efficiency TPV conversion. For a far-field TPV system without any enhancement, sub-bandgap suppression is more important than the superbandgap emissivity. Our analysis showed that the optimum bandgap is determined by the emitter temperature, sub-bandgap suppression, superbandgap enhancement, and PV heating. Using an optimum bandgap PV cell, the TPV system can achieve efficiencies of over 60% of Carnot's limit only when both sub-bandgap suppression and superbandgap enhancement are employed. This analysis shows that with proper engineering, currently used refractory optical materials can reach conversion efficiencies well beyond 25% and 50% of Carnot's limit in the far- and near-field operations, respectively.

Further higher efficiency requires better refractory plasmonic materials, and a-SWCNTs are a promising material platform. The findings of this study serve as guidelines toward a practical design of highefficiency TPV system.

This material is based upon work supported by the National Science Foundation under Grant No. ECCS-1935446.

REFERENCES

- ¹M. Laroche, R. Carminati, and J.-J. Greffet, J. Appl. Phys. 100, 063704
- ²V. B. Svetovoy and G. Palasantzas, Phys. Rev. Appl. 2, 034006 (2014).
- ³D. N. Woolf, E. A. Kadlec, D. Bethke, A. D. Grine, J. J. Nogan, J. G. Cederberg, D. Bruce Burckel, T. S. Luk, E. A. Shaner, and J. M. Hensley, Optica 5, 213
- ⁴J. I. Watjen, X. L. Liu, B. Zhao, and Z. M. Zhang, Micro/Nanoscale Thermal Radiation; Micro/Nanoscale Energy Devices and Systems (ASME, 2016), Vol. 1, p. V001T05A011.

 5K. Park, S. Basu, W. King, and Z. Zhang, J. Quant. Spectrosc. Radiat. Transfer
- 109, 305 (2008).
- ⁶B. Zhao, K. Chen, S. Buddhiraju, G. Bhatt, M. Lipson, and S. Fan, Nano Energy 41, 344 (2017).
- ⁷R. St-Gelais, G. R. Bhatt, L. Zhu, S. Fan, and M. Lipson, ACS Nano 11, 3001
- ⁸B. Wernsman, R. Siergiej, S. Link, R. Mahorter, M. Palmisiano, R. Wehrer, R. Schultz, G. Schmuck, R. Messham, S. Murray, C. Murray, F. Newman, D. Taylor, D. DePoy, and T. Rahmlow, IEEE Trans. Electron Devices 51, 512
- ⁹T. Burger, D. Fan, K. Lee, S. R. Forrest, and A. Lenert, ACS Photonics 5, 2748
- 10Z. Omair, G. Scranton, L. M. Pazos-Outón, T. P. Xiao, M. A. Steiner, V. Ganapati, P. F. Peterson, J. Holzrichter, H. Atwater, and E. Yablonovitch, Proc. Nat. Acad. Sci. U. S. A. 116, 15356 (2019).
- 11 E. Rephaeli and S. Fan, Opt. Express 17, 15145 (2009).
- ¹²Z. Hu, Y. Zhang, L. Liu, L. Yang, and S. He, Prog. Electromagn. Res. 162, 95 (2018).
- ¹³M. Whale and E. Cravalho, IEEE Trans. Energy Convers. 17, 130 (2002).
- ¹⁴T. Asano, M. Suemitsu, K. Hashimoto, M. De Zoysa, T. Shibahara, T. Tsutsumi, and S. Noda, Sci. Adv. 2, e1600499 (2016).
- ¹⁵M. Shimizu, A. Kohiyama, and H. Yugami, J. Photonics Energy 5, 053099 (2015).
- 16D. M. Bierman, A. Lenert, W. R. Chan, B. Bhatia, I. Celanović, M. Soljačić, and E. N. Wang, Nat. Energy 1, 16068 (2016).
- ¹⁷C. Simovski, S. Maslovski, I. Nefedov, and S. Tretyakov, Opt. Express 21, 14988 (2013).

- 18C.-C. Chang, W. J. M. Kort-Kamp, J. Nogan, T. S. Luk, A. K. Azad, A. J. Taylor, D. A. R. Dalvit, M. Sykora, and H.-T. Chen, Nano Lett. 18, 7665 (2018).
- ¹⁹Y. Nam, Y. X. Yeng, A. Lenert, P. Bermel, I. Celanovic, M. Soljačić, and E. N. Wang, Sol. Energy Mater. Sol. Cells 122, 287 (2014).
- ²⁰A. Lenert, Y. Nam, D. M. Bierman, and E. N. Wang, Opt. Express 22, A1604
- ²¹A. Datas and C. Algora, Prog. Photovoltaics: Res. Appl. 21, 1040 (2013).
- ²²A. Datas, Sol. Energy Mater. Sol. Cells **134**, 275 (2015).
- 23S. McSherry, T. Burger, and A. Lenert, J. Photonics Energy 9, 1 (2019).
- ²⁴G. T. Papadakis, S. Buddhiraju, Z. Zhao, B. Zhao, and S. Fan, preprint arXiv:1909.08701 (2019).
- ²⁵C. F. Doiron and G. V. Naik, J. Opt. **20**, 084001 (2018).
- ²⁶Z. Yu, N. P. Sergeant, T. Skauli, G. Zhang, H. Wang, and S. Fan, Nat. Commun. 4, 1730 (2013).
- ²⁷A. Fiorino, L. Zhu, D. Thompson, R. Mittapally, P. Reddy, and E. Meyhofer, Nat. Nanotechnol. 13, 806 (2018).
- ²⁸S. Molesky and Z. Jacob, Phys. Rev. B **91**, 205435 (2015).
- ²⁹M. Lim, J. Song, J. Kim, S. S. Lee, I. Lee, and B. J. Lee, J. Quant. Spectrosc. Radiat. Transfer 210, 35 (2018).
- 30 A. Karalis and J. D. Joannopoulos, Sci. Rep. 6, 28472 (2016).
- ³¹K. Chen, P. Santhanam, and S. Fan, Appl. Phys. Lett. **107**, 091106 (2015).
- 32H. Yu, D. Liu, Y. Duan, and Z. Yang, J. Quant. Spectrosc. Radiat. Transfer 217, 235 (2018).
- 33Y. Guo, S. Molesky, H. Hu, C. L. Cortes, and Z. Jacob, Appl. Phys. Lett. 105, 073903 (2014).
- 34W. T. Chen, A. Y. Zhu, V. Sanjeev, M. Khorasaninejad, Z. Shi, E. Lee, and F. Capasso, Nat. Nanotechnol. 13, 220 (2018).
- 35S. Shrestha, A. C. Overvig, M. Lu, A. Stein, and N. Yu, Light: Sci. Appl. 7, 85 (2018).
- 36 T. Roy, E. T. F. Rogers, and N. I. Zheludev, Opt. Express 21, 7577 (2013).
- 37M. Buljan, J. Mendes-Lopes, P. Benítez, and J. C. Miñano, J. Photonics Energy 4, 040995 (2014).
- ³⁸K. Shanks, S. Senthilarasu, and T. K. Mallick, Renew. Sustain. Energy Rev. **60**, 394 (2016).
- ³⁹S. Fray, F. Johnson, and J. Quarrington, in *Lattice Dynamics: Proceedings of the* International Conference Held at Copenhagen, edited by R. Wallis (Pergamon, 1965), pp. 377-379.
- ⁴⁰O. D. Miller, E. Yablonovitch, and S. R. Kurtz, IEEE J. Photovoltaics 2, 303
- ⁴¹G. V. Naik, V. M. Shalaev, and A. Boltasseva, Adv. Mater. 25, 3264 (2013).
- 42W. Gao, C. F. Doiron, X. Li, J. Kono, and G. V. Naik, ACS Photonics 6, 1602 (2019).
- ⁴³P. West, S. Ishii, G. Naik, N. Emani, V. Shalaev, and A. Boltasseva, Laser Photonics Rev. 4, 795 (2010).
- 44M. Minissale, C. Pardanaud, R. Bisson, and L. Gallais, J. Phys. D: Appl. Phys. **50**, 455601 (2017).
- 45 P. Romaniello, P. L. de Boeij, F. Carbone, and D. van der Marel, Phys. Rev. B 73, 075115 (2006).